Search for disoriented chiral condensate at the Fermilab Tevatron

T. C. Brooks,* M. E. Convery,† W. L. Davis, K. W. Del Signore,‡ T. L. Jenkins, E. Kangas,§ M. G. Knepley,‖
K. L. Kowalski, and C. C. Taylor
Department of Physics, Case Western Reserve University, Cleveland, Ohio 44106-7079

S. H. Oh and W. D. Walker
Department of Physics, Duke University, Durham, North Carolina 27708-0305

P. L. Colestock, B. Hanna, M. Martens, and J. Streets¶
Fermi National Accelerator Laboratory, P.O. Box 500, Batavia, Illinois 60510

R. C. Ball, H. R. Gustafson, L. W. Jones, and M. J. Longo
Department of Physics, University of Michigan, Ann Arbor, Michigan 48109-1120

J. D. Bjorken
Stanford Linear Accelerator Center, Stanford, California 94309

A. Abashian and N. Morgan
Department of Physics, Virginia Polytechnic Institute, Blacksburg, Virginia 24061-0435

C. A. Pruneau
Department of Physics and Astronomy, Wayne State University, Detroit, Michigan 48202

We present results from MiniMax (Fermilab T-864), a small test/experiment at the Fermilab Tevatron designed to search for the production of a disoriented chiral condensate (DCC) in $p\text{-}\bar{p}$ collisions at $\sqrt{s} = 1.8$ TeV in the forward direction, $\sim 3.4 < \eta < \sim 4.2$. Data, consisting of 1.3×10^6 events, are analyzed using the robust observables developed in an earlier paper. The results are consistent with generic, binomial-distribution partition of pions into charged and neutral species. Limits on DCC production in various models are presented.

I. INTRODUCTION

The purpose of the MiniMax test/experiment (T-864) at the Fermilab Tevatron as set out in its proposal was to (1) demonstrate the feasibility of operating spectrometers in the hostile environment of the far-forward, small angle region in high-energy hadron colliders, (2) search for the presence of disoriented chiral condensate (DCC) and possibly related exotic phenomena such as Centauro events, and (3) contribute data on inclusive spectra and multiplicity distributions in an unexplored region of phase space [1,2]. The experiment was proposed in April 1993, commissioned by January 1994, and upgraded in several stages during the next two years. The data reported here were acquired in January 1996.

---

*Now at Department of Physics, Stanford University, Stanford, CA 94305.

†Now at The Rockefeller University, New York, NY 10021.

‡Now at Department of Physics, University of Michigan, Ann Arbor, MI 48109-1120.

§Now at Department of Physics, Massachusetts Institute of Technology, Cambridge, MA 02139.

‖Now at Department of Computer Science, University of Minnesota, Minneapolis, MN 55455.

¶Now at Lucent Technologies.

The principal purpose of this paper is to report the results of our DCC search. A signal for the formation and decay of disoriented chiral condensates [3,4] in hadronic and heavy-ion collisions is an anomalous joint multiplicity distribution of neutral and charged secondary pions, reflected in the probability density

$$P(f)_{DCC} = \frac{1}{2\sqrt{f}}, \tag{1}$$

where f is the fraction of the total number of pions which are neutral. (There are a variety of proposed mechanisms other than DCC's which might also lead to this distribution [5]. We will not hereafter explicitly make this distinction.) Note that the distribution, Eq. (1), differs markedly from the "generic," binomial partition of pions into charged and neutral species expected from ordinary production mechanisms.

Neutral pions were not reconstructed in this experiment. Instead, we studied the joint multiplicity distribution of charged particles and gamma rays. In a recent publication [6], we showed that robust observables can be constructed from such data which still contain much of the information in Eq. (1) regarding the presence (or absence) of DCC's. It is this method which we apply to the MiniMax data.

The basic detector requirements of a DCC search, then, are to be able to count, event by event, the number of charged particles and photons in a given acceptance. The detailed design of the MiniMax detector was determined by a variety of considerations. The far-forward direction of production angles less than ~ 50 mrad was chosen because cosmic ray data provide hints of novel phenomena in this region of phase space, and because it is largely unexplored at hadron colliders. In this region it is necessary to determine carefully the production angles of charged particles and the conversion products of photons. We therefore designed a forward spectrometer with a large number of planes of multiwire proportional chambers (MWPC's). A plane of Pb converter located within the spectrometer permitted the identification of photons through their conversion products. An electromagnetic calorimeter placed behind the spectrometer provided additional information.

The acceptance of the spectrometer was quite small. This was due to a combination of fiscal and physical constraints, together with theoretical considerations regarding the possible size of DCC domains. Available resources dictated the choice of MWPC's as the detector technology. Once this choice had been made, the cramped environment of the detector dictated the acceptance: there was no space for additional detection elements. The resulting fiducial region of the MiniMax detector was only $\Delta\eta\Delta\phi\approx0.75$. (It is amusing to note that this corresponds to about 0.75 sr in a reference frame in which the axis of the detector is boosted to 90° with respect to the beam axis.) Nevertheless, this choice of acceptance is consistent with the consideration that the correlation length of the DCC chiral order parameter may be so small that even large acceptance detectors should be subdivided into cells of the order of the MiniMax acceptance in order to avoid averaging out the DCC effects.

The detector elements were modular and portable which permitted efficient maintenance, modifications and upgrades during the extremely limited periods of access to the detector. In the development period from 1993–1996, the number of MWPC's was increased from an initial 8, first to 12, then to 16, and finally to 24 planes as the need for additional redundancy became clear. The entire detector was removed and rebuilt 3 times during this period. Early running demonstrated the need for a special beam pipe to improve resolution and decrease backgrounds. This beam pipe was commissioned in 1995. The original choice of large-angle stereo for the MWPC's was also changed in 1995 to small-angle stereo in order to improve pattern recognition capability, thereby reducing the number of spurious track candidates though with some loss of resolution.

It was also recognized during the development period that it was possible to add simple detection elements in the opposite hemisphere which provided tags of the presence of leading or diffractively produced (anti)baryons in each event. These tagging detectors were installed and tested in 1995 and worked with demonstrably high purity during the data runs.

The detector, as it was configured during the data runs reported here, is described in more detail in the next section. Section III describes the analysis chain from track finding through the determination of the joint multiplicity distribution of charged particles and converted photons. Section IV reviews the use of robust observables to search for the presence of DCC in the data. The results are presented in Sec. V. Section VI contains a summary and our conclusions.

II. DETECTOR

A. Apparatus

The MiniMax detector was located at the C0 region of the Fermilab Tevatron. The final configuration of the detector, used for acquisition of the data reported here, is illustrated in Figs. 1 and 2. The salient parts of the apparatus are the beam pipe, the MWPC tracking telescope including a remotely movable Pb converter, the trigger scintillator, the electromagnetic calorimeter, and the upstream (in the sense of proton motion in the Tevatron) tagging detectors.

Early running during the MiniMax development period confirmed the need for a special beam pipe. Two considerations governed the design: the need for a ''thin'' window to minimize interactions of particles before reaching the detector and the need to minimize backgrounds created by particles outside the acceptance, particularly at higher η, interacting with the beam pipe and showering. The design of this special beam pipe and vacuum tank was complicated by the fact that the Tevatron abort system was also located at C0.

The general features of this special beam pipe are illustrated in Fig. 1. All elements of this beam pipe were constructed from aluminum. The large central vacuum tank ensured that there was no material within 12 cm of the collision point. This tank terminated on the detector side in an aluminum plate, which provided transitions to both the Tevatron beam pipe and the abort pipe. The MWPC tracking telescope viewed the collision region through a circular window 22.86 cm in diameter and 0.64 cm in thickness milled into this plate. In the region of the MWPC's, the Tevatron beam pipe was flared in a stepped cylindrical fashion using aluminum tubing of varying radii and thickness 0.76 mm. In this way, interactions of forwardly produced particles with the beam pipe were localized in pseudorapidity.

Tracking information was provided by 24 MWPC's. Each chamber had 128 wires with spacing 2.54 mm and an active area of approximately 32.5 cm $\times$ 32.5 cm. Their construction was similar to those described by Bevington *et al.* [7]. The chambers operated on a mixture of 80% Ar and 20% CO_2. Two types of readout electronics were used: half the chambers were read out with latch-only information, and the other half recorded the magnitude of the charge deposited on each wire.

The forward eight chambers served to identify charged particles coming from the collision vertex. This was followed by 1 X_0 of Pb converter which could be moved by remote control into and out of the detector acceptance. This was followed by 16 more MWPC's which served to identify gamma ray conversion products and improve the resolution of charged particles.

The MWPC planes were perpendicular to the beam line and oriented so as to provide three-dimensional positions of all tracks traversing the detector in a single event. Considerable effort went into optimizing the orientation of the cham-
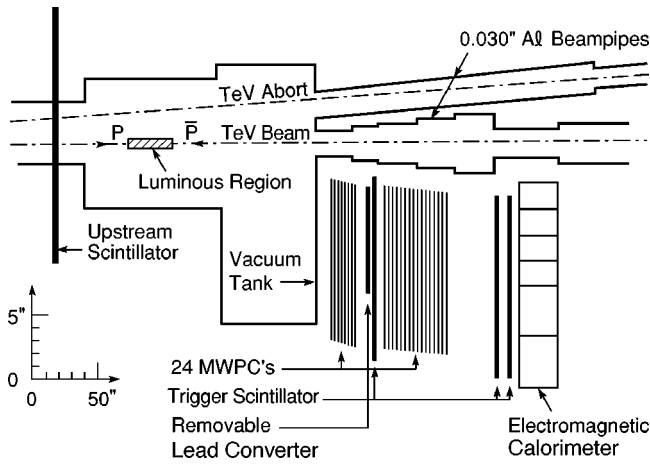
FIG. 1. Plan view of the final configuration of the MiniMax detector, illustrating the tracking detectors, the beam pipe architecture and the location of the trigger scintillator elements.
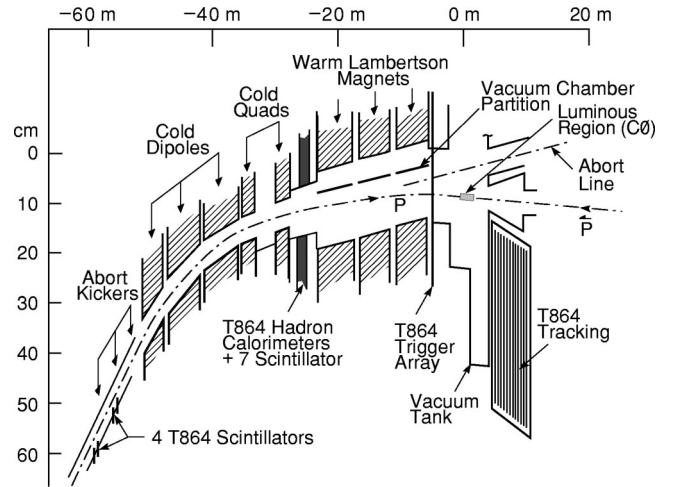

FIG. 2. Plan view of the final configuration of the MiniMax detector illustrating the incorporation of detector elements amidst the Tevatron magnets in order to obtain leading particle and diffractive tags in the downstream $\bar{p}$ direction.

bers with respect to redundancy, resolution and pattern recognition. In describing the final orientation of the MWPC's, it is convenient to introduce a coordinate system in which the z axis is along the Tevatron beam, the u axis is perpendicular to the beam and points towards the center line of the detector, and the v axis is orthogonal to the other two. Three of the eight chambers located in front of the Pb converter were oriented with their wires parallel to the v axis, two at $\pm 15°$ to this direction, and the remaining three with their wires at $\pm 15°$ and parallel to the u direction. Behind the Pb converter, every other chamber was oriented with its wires parallel to the v axis. The remaining chambers were oriented at various angles but always within $\pm 15°$ of the v direction. This arrangement, with 11 of the 24 chambers having parallel wires, permitted simple visualization and formed the basis for one of the two track reconstruction algorithms used for analysis.

The array of 28 lead-scintillator electromagnetic calorimeter modules, located behind the MWPC tracking system, provided information on photons and showering charged particles traversing the apparatus. This information has been useful for a variety of diagnostic purposes. Pattern recognition proved to be difficult, however, because of the rather coarse angular resolution and the rather large background levels. The data from this system have not been directly incorporated into the analysis presented here.

Figure 2 illustrates the detectors installed within the Tevatron lattice in order to tag leading particles and diffractive events. The presence of the Lambertson abort magnets ensured that particles leaving the collision area in the direction opposite the main detector would traverse a magnetic field within a comparatively large aperture beam pipe. Fortuitously, there was approximately 2 m of free space between the Lambertson magnets and the quadrupole magnets in which it was possible to position two 10 cm×10 cm×117 cm lead-scintillator hadron calorimeter modules, one on each side of the beam pipe. One module thus saw zero-degree neutral particles from the collision region, albeit with a small acceptance and through approximately one interaction length of material. Forward-produced negatively charged particles

of $x \sim 0.5$ were bent into the other module. Several pieces of scintillator provided additional information useful in characterizing these events. Four scintillation counters were also placed adjacent to the beam pipe in the vicinity of the abort kicker magnets, approximately 60 m upstream. The magnetic architecture of the C0 straight section was such that antiprotons of $x \sim 0.9$ exited the beam pipe in this region. The scintillation counters detected the resulting showers.

B. Operating conditions, trigger and rates

A hodoscope composed of eight scintillation counters arranged in a square array 47 cm on a side and 2.5 cm thick with a 16.5 cm square aperture was centered on the 15.24 cm beam pipe at $z = -194$ cm. (The location of this hodoscope is indicated by ''upstream scintillator'' in Fig. 1.) Immediately behind the Pb converter, two scintillation counters, each 20.3 cm×40.6 cm×1.27 cm, were mounted together to form a square region covering the acceptance of the MWPC's. Two additional arrays of the same size were mounted immediately behind the final MWPC. The trigger required a coincidence of hits with appropriate timing in the hodoscope, in the array immediately behind the converter and in the final array, together with a beam-crossing time signal provided by the accelerator. The experiment was gated off during Main ring acceleration periods because of high backgrounds.

The trigger cross section was quite large despite the small acceptance of the detector, owing to the large amount of material near the collision point (such as the Tevatron beam pipe, the Main Ring, the floor, etc.) which efficiently generated secondary shower products. The actual trigger cross section was estimated to be 43 mb. This was determined from the Collider Detector at Fermilab (CDF) measured inelastic cross section [8], the real-time observed D0 luminosity, the MiniMax trigger rate, and the ratio of the β functions between the C0 and D0 collision regions, including corrections for finite bunch length and bunch-to-bunch intensity varia-

tions. Detailed GEANT simulations of the detector and its environment [2] were consistent with the observed trigger cross section. A small fraction of the events ($\sim 1.4\%$) were associated with high-mass diffractive dissociation of the antiproton.

Under ordinary operation during run IB of the Tevatron, the beams at C0 were separated by electrostatic separators, and no collisions occurred in the C0 collision area. MiniMax commissioning was done during special runs, typically at the ends of stores when the beams were scraped down to sufficiently low intensities to permit the separators to be turned off. The data reported here were taken during six days of special low-luminosity running during January 1996. Data, consisting of 1.3×10^6 events taken with the Pb converter in the acceptance of the detector, are analyzed in the remainder of this paper. The luminosity at the C0 collision point was inferred from the D0 luminosity corrected for differences in the magnetic architecture at the two points and the fact that bunches that collide at C0 are not the same pairs that collide at D0. The C0 luminosity during these runs ranged from about 10^{26} cm^{-2} s^{-1} to about 10^{28} cm^{-2} s^{-1}. Triggers in these runs occurred at rates from a few Hz up to about 75 Hz. As a result of dead time, events were only recorded at about 40% of the trigger rate at the higher luminosities; essentially every event was recorded at the lower luminosities. Additional data, including data with the Pb converter outside of the acceptance, were also taken during this period, but are not directly used in this analysis.

C. Backgrounds

The detector was located very close to the beam line and as a consequence events typically showed many reporting wires in the MWPC's. The median number of reporting wires per event was 210, or 6.8% of the total number of wires. The background was not uniformly distributed; wires closer to the beam had a higher probability of reporting than wires farther away. The distribution of reporting wires could be modeled reasonably well by asuming that for any single event, the density per unit area of ionizing tracks was A/r, with r the perpendicular distance from the beam. The parameter A varied from 0.12 cm^{-1} in the front chamber to 0.31 cm^{-1} in the rear chamber. Most of these hits were not associated with tracks from the collision vertex. Visual examination of the events showed that in many cases, multiple tracks entered the chambers from the adjacent beam pipe. Not all reporting wires were obviously associated with tracks.

Operation under a broad range of conditions provided clear evidence that these backgrounds were correlated with secondaries produced in the proton-antiproton collision of interest, and were not associated with beam-gas interactions. In the runs reported in this paper, the beam-gas trigger rate was always less than 5% of the collision trigger rate.

The GEANT simulations of the experiment and its environment reproduced the general form of the distribution of hit wires, but consistently underestimated their number giving values that were about 60% of the actual number in the front of the spectrometer to about 50% in the rear. Great effort was expended, without much success, in attempting to understand the discrepancy. Similar discrepancies have been noted in other uses of similar chambers, where it has been suggested that the discrepancy is due to protons knocked out of the mylar window of the MWPC by very low energy neutrons, which may not be well modeled by GEANT [9].

III. JOINT MULTIPLICITY DISTRIBUTIONS OF CHARGED PARTICLES AND CONVERTED PHOTONS

A. Algorithms for finding charged particles and photons

The output of the MWPC's is, for each event, a list of wires reporting hits. From this it is necessary to reconstruct the number of charged particles and converted gamma rays within the acceptance of the detector arising from the proton-antiproton collision. There are two principal stages of this analysis: the identification of track segments and the matching of track segments at the Pb converter in order to identify converted gamma rays and through-going charged tracks.

While both tasks are essential, the first, the identification of track segments, is particularly critical because of the large number of background hits. In particular, at very high occupancies, spurious tracks arising from the accidental juxtaposition of hit wires became a serious problem. In practice, events with more than 600 wires (20%) reporting have been eliminated from the analysis reported in this paper for this reason. This is approximately 3% of the total data set. In order to assess systematic effects arising from these considerations, MiniMax developed two distinct trackers. While both algorithms are rather intricate in their details, it is worth briefly reviewing the basic principles underlying each of them.

The principal tracker, which we will refer to as the "combinatorial tracker" in the remainder of this paper, used various combinations of four non-parallel "cross-hair" chambers to define candidate tracks. The other chambers were then searched for confirming hits. If the resulting collection of wire hits satisfied suitable track quality criteria, it was declared a track segment, with parameters determined by a least-squares fit.

The second track reconstruction algorithm, which we shall refer to as the "u-v" tracker in the remainder of this paper, exploited the power of the 11 chambers with parallel wires (in the v direction). Track candidates were first identified in this projection. The algorithm then examined the perpendicular plane through the candidate track, checking for candidate trajectories in this projection, which had significantly poorer resolution due to the small angle stereo in the rear chambers. If suitable track quality criteria were satisfied, the parameters of the track that passed through the sensitive area of those wires identified with the track were determined by a simplex linear programming algorithm. We will present selected results from this track reconstruction algorithm to illustrate systematics; our principal results are based on the combinatorial tracker unless otherwise noted.

The output of the track reconstruction algorithms were then used to determine the number of charged particles and converted gamma rays from the interaction region entering the fiducial region of the MWPC tracking telescope. Charged
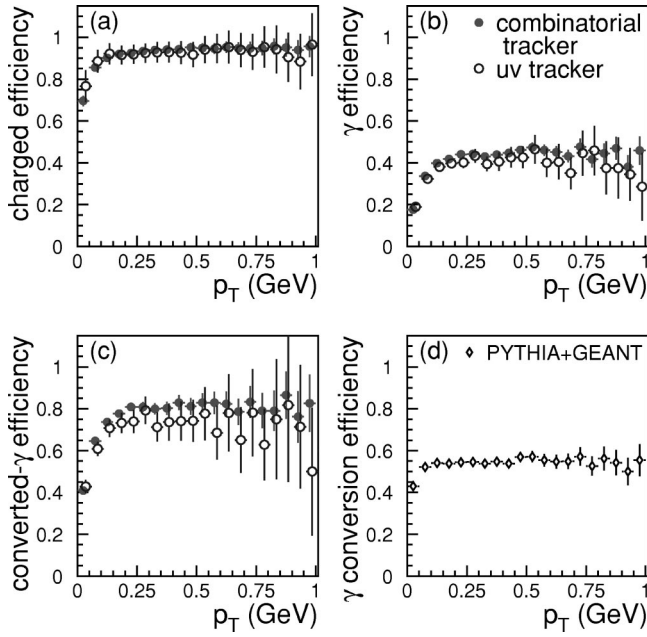
FIG. 3. PYTHIA+GEANT efficiency estimates for both combinatorial and u-v track-finding algorithms. (a) The efficiency for finding charged particles as a function of p_t. (b) The over-all efficiency for finding photons as a function of p_t. (c) The efficiency for finding photons known to have converted, as a function of p_t. (d) The efficiency for photons to convert, as a function of p_t.

tracks were identified as track segments in the front chambers that matched track segments in the rear chambers at the Pb converter. One or more tracks in the rear chambers appearing to emerge from a common point on the Pb converter, without a matching track segment in the front chambers, were identified as conversion products, and the group was counted as a converted gamma ray. The algorithm includes a number of cuts which were developed and which are described in detail in [2].

One point worth noting is that the algorithms for vertex fitting at the converter were developed after the bulk of the work on the combinatorial tracker had been completed, and the various cuts were developed on the basis of the output of that tracker, on both real data and the Monte Carlo simulation to be described shortly. The u-v tracker was developed after the vertex algorithms were mature, and no effort was made to retune the various cuts in these algorithms.

B. Algorithm performance

The assessment of the algorithms for track reconstruction and vertex fitting at the converter is complicated by the fact that the Monte Carlo simulation significantly underestimated the density of hit wires, as described above. This means that estimates based on Monte Carlo simulations of efficiencies for identifying the various species of particles cannot necessarily be quantitatively trusted. Fortunately, as described in the next section, the actual MiniMax DCC search relies on techniques which are insensitive to these quantities. Nevertheless, it is worthwhile to briefly describe the performance of the algorithms as understood from the Monte Carlo simulation.
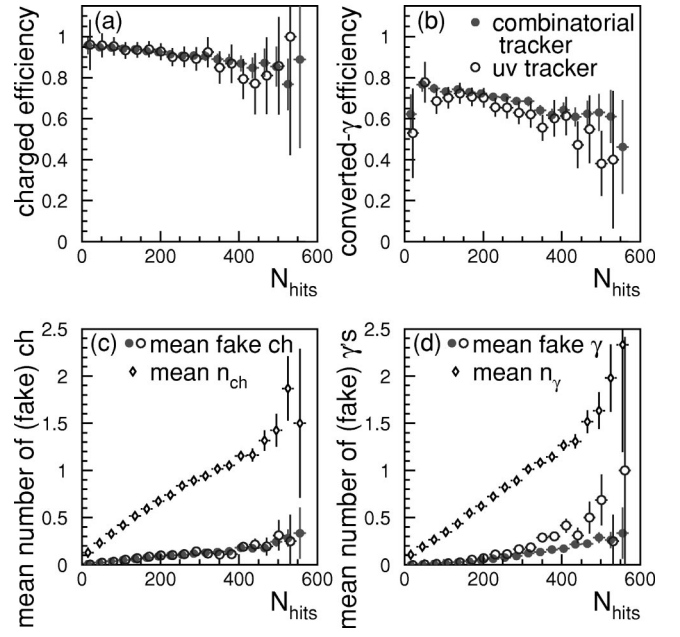

FIG. 4. PYTHIA+GEANT efficiency and ''fake'' estimates for both combinatorial and u-v track-finding algorithms as a function of N_{hits}, the number of wire hits reported in the event. (a) The efficiency for finding charged particles as a function of N_{hits}. (b) The efficiency for finding converted photons as a function of N_{hits}. (c) The mean number of correctly identified and ''fake'' charged particles found, as a function of N_{hits}. (d) The mean number of correctly identified and ''fake'' converted photons found, as a function of N_{hits}.

The details of our use of the standard PYTHIA event generator [10] and of the GEANT detector simulation package [11], together with a description of our Monte Carlo DCC generator, have been described elsewhere [6,2]. Here we discuss using these tools to assess how well our algorithms identify tracks that represent charged particles or converted photons originating in the primary collision, as distinguished from secondary and spurious, i.e., fake, tracks.

The efficiencies are calculated by comparing reconstructed charged tracks and photons with those known to be present in the PYTHIA-GEANT events. The actual charged tracks are defined as charged particles from PYTHIA which are aimed into the acceptance, while converted photons are defined in terms of $e^{\pm}$ tracks in GEANT which originate in the region between the front and rear groups of MWPC's, hit at least 14 of the 16 rear MWPC's, and can be matched to a PYTHIA photon. A charged track or photon is said to be found if one is reported in the tracking output within a small distance of the actual track at the converter plane.

Reconstructed tracks that do not match up with actual tracks are declared to be fakes. A minimum bias sample of PYTHIA-GEANT events was scanned to determine the sources of such fakes. Most fake charged tracks were secondary particle tracks from decays. Particles resulting from interactions in the detector and its environment were also significant. Less than 1% of the ''fake'' charged tracks appeared to be genuinely spurious. ''Fake'' photons arise for similarly diverse reasons.
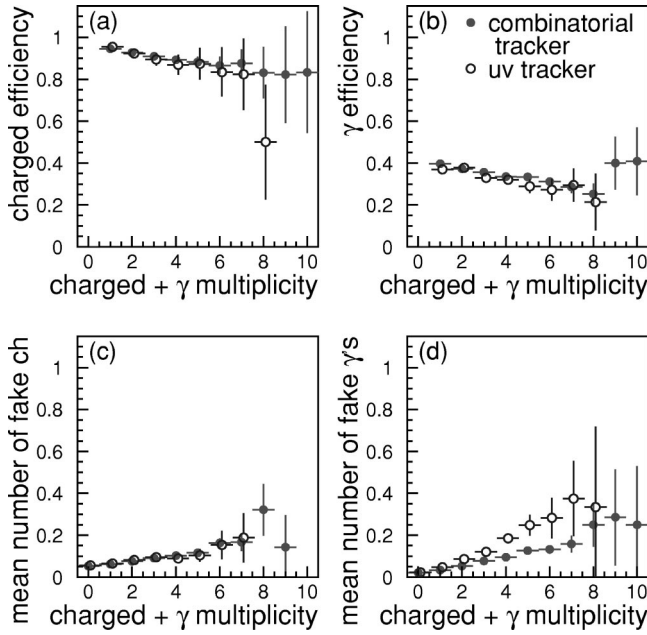
FIG. 5. PYTHIA+GEANT efficiency and ''fake'' estimates for both combinatorial and u-v track-finding algorithms as a function of total multiplicity into the acceptance. (a) The efficiency for finding charged particles as a function of total multiplicity into the acceptance. (b) The efficiency for finding photons as a function of total multiplicity into the acceptance. (c) The mean number of ''fake'' charged particles found as a function of total multiplicity into the acceptance. (d) The mean number of ''fake'' photons found as a function of total multiplicity into the acceptance.

We now summarize the results of these studies.

DCC production is often thought to be characterized by low $\langle p_t \rangle$, so it is important that we maintain good efficiencies for finding charged particles and converted gammas in this region. These efficiencies are plotted in Fig. 3. Good efficiencies for both charged particles and photons are maintained to p_t below 100 MeV/c.

As noted above, a great concern is the performance of the reconstruction algorithms as chamber occupancies become large. Figure 4 illustrates the performance of the algorithms for correctly identifying charged particles and photons as a function of N_{hits}, the number of wires reporting hits in the event. Efficiencies are high, and the mean number of ''fakes'' is significantly smaller than the mean number of correctly identified particles. It should be noted that the u-v tracker is comparable to the combinatorial tracker in identifying charged particles, but seems to have lower efficiencies for correctly finding converted photons and a significantly enhanced probability of finding ''fake'' photons at high occupancies.

Figure 5 similarly illustrates the performance of the algorithms as a function of the total multiplicity into the acceptance.

As noted above, occupancies in the MWPC's vary as A/r and so are much higher near the beam pipe, that is at higher pseudorapidity, η. Figure 6 illustrates that the performance of the reconstruction algorithms is reasonably uniform over the entire acceptance.
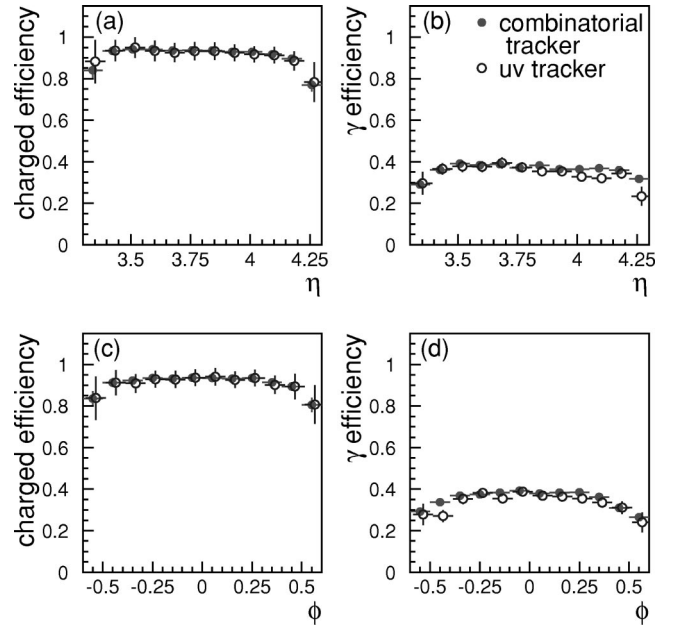

FIG. 6. PYTHIA+GEANT efficiency estimates for both combinatorial and u-v track-finding algorithms as a function of pseudorapidity η and azimuthal angle ϕ. (a) The efficiency for finding charged particles as a function of η. (b) The efficiency for finding converted photons as a function of η. (c) The efficiency for finding charged particles as a function of ϕ. (d) The efficiency for finding photons as a function of ϕ.

C. Joint distributions of charged particles and photons

We now present the basic experimental data of MiniMax: the observed joint distributions of charged particles and converted photons within our acceptance. The data presented are based on the output of the combinatorial tracking algorithm unless otherwise noted. We first present minimum bias data, and then data sets defined by various tags.

Table I presents the observed minimum bias joint distribution of charged particles and converted photons. This will be the basis for our DCC search in minimum bias events.

It has been suggested that DCC-like phenomena might occur preferentially in diffractive events [12]. To test for this, MiniMax identified the subset of the data in which the

TABLE I. The number of events observed with a given n_{ch}, n_γ: minimum bias data set.

		n_γ								
		0	1	2	3	4	5	6	7	8
	0	742039	111976	14868	2237	401	60	9	8	1
	1	318521	56182	9324	1557	258	49	11	1	0
	2	78220	17232	3204	573	139	27	3	0	0
	3	16018	4321	912	184	32	8	0	0	0
n_{ch}	4	3021	856	197	43	8	2	0	0	0
	5	473	170	46	7	4	0	0	0	0
	6	76	34	5	2	0	0	0	0	0
	7	10	5	1	0	0	0	0	0	0
	8	0	1	0	0	0	0	0	0	0

TABLE II. The observed number of events with a given n_{ch}, n_γ, in which there is a leading antiproton of $x \sim 0.9$.

		n_γ								
		0	1	2	3	4	5	6	7	8
	0	11224	1532	188	25	7	0	0	0	0
	1	4245	622	97	10	2	1	0	0	0
	2	798	173	27	8	0	0	0	0	0
	3	145	39	5	2	0	0	0	0	0
n_{ch}	4	13	5	2	0	1	0	0	0	0
	5	6	2	1	0	0	0	0	0	0
	6	0	0	0	0	0	0	0	0	0
	7	0	0	0	0	0	0	0	0	0
	8	0	0	0	0	0	0	0	0	0

TABLE IV. The observed number of events with a given n_{ch}, n_γ in which there is a leading zero degree neutral particle.

		n_γ								
		0	1	2	3	4	5	6	7	8
	0	14313	1944	244	37	5	1	0	0	0
	1	5439	871	139	22	2	2	0	0	0
	2	1138	232	42	6	0	0	0	0	0
	3	215	41	9	3	0	0	0	0	0
n_{ch}	4	31	9	1	1	0	0	0	0	0
	5	5	3	2	0	0	0	0	0	0
	6	0	0	0	0	0	0	0	0	0
	7	0	0	0	0	0	0	0	0	0
	8	0	0	0	0	0	0	0	0	0

scintillation counters in the vicinity of the kicker magnets at ~ 60 m upstream fired, indicating a leading antiproton with $x \sim 0.9$. The joint multiplicity distribution in this class of events ("diffractive-$\bar{p}$" events) is presented in Table II.

The hadron calorimeter modules located ~ 25 m upstream permitted MiniMax to isolate a subset of the data characterized by leading antiprotons of $x \sim 0.5$ (forward-$\bar{p}$ events) and by leading zero-degree neutrals (forward-$\bar{n}$ events). The joint multiplicity distributions are presented in Table III and Table IV, respectively.

Many models for DCC formulation suggest that there should be a correlation with total event multiplicity. In order to avoid biasing the data, it is important to cut on multiplicity in a manner that does not depend on what is seen in the event within the MiniMax MWPC acceptance. Fortunately, the scintillator hodoscope on the opposite side of the collision vertex provides such a tool. Peaks in the ADC spectrum of each scintillation counter provided a calibration in terms of the number of minimum ionizing particles passing through the hodoscope. The data set was then subdivided into ten bins of increasing multiplicity in the hodoscope, with an equal number of events in each bin. Despite being some 7 units of pseudorapidity away from the fiducial region for tracking, there is a clear correlation between multiplicity in the hodoscope and the number of particles observed by the

TABLE III. The observed number of events with a given n_{ch}, n_γ in which there is a leading antiproton of $x \sim 0.5$.

		n_γ								
		0	1	2	3	4	5	6	7	8
	0	21447	3068	403	58	16	1	0	0	0
	1	8594	1439	219	34	5	0	0	0	0
	2	1795	391	83	15	2	0	0	0	0
	3	334	80	23	2	2	0	0	0	0
n_{ch}	4	61	18	5	1	0	1	0	0	0
	5	5	7	0	0	0	0	0	0	0
	6	2	1	0	0	0	0	0	0	0
	7	0	0	0	0	0	0	0	0	0
	8	0	0	0	0	0	0	0	0	0

tracking system. This is illustrated in Fig. 7. Tables V and VI present the joint multiplicity distributions for events with energy deposition in the hodoscope of less than 2.5 mips (minimum ionizing particles) and more than 34 mips, respectively.

Finally, Fig. 8 presents the inclusive distributions $dN_{ch}/d\eta$ and $dN_\gamma/d\eta$, uncorrected for detection and trigger efficiencies. For comparison purposes, distributions from PYTHIA and the output of our entire PYTHIA-GEANT-tracking-reconstruction chain are also plotted.

IV. DCC SEARCH

A. General strategy

The output of the analysis chain described in the previous section is, for each experimental run, a table of observed
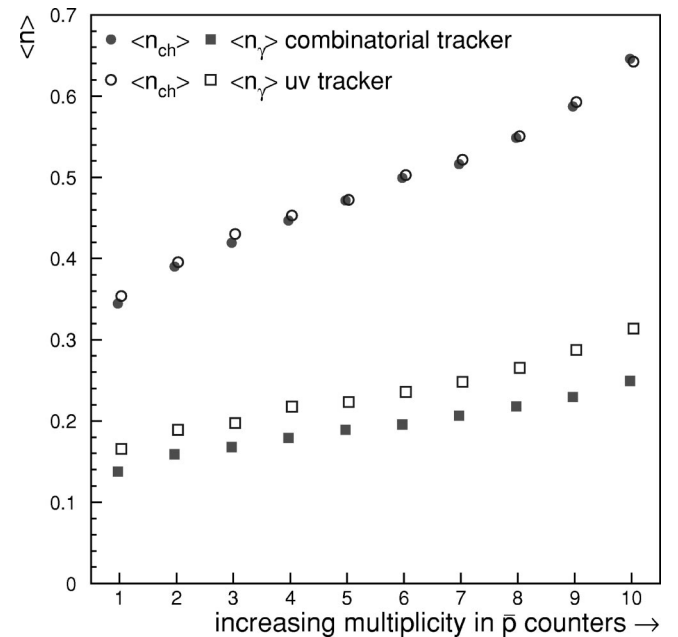

FIG. 7. Correlations between multiplicity as seen by MiniMax tracking and multiplicity seen in the scintillator hodoscope. Events were grouped in bins by multiplicity observed in the scintillator hodoscope such that each bin contains 10% of the data.

TABLE V. Number of events with a given n_{ch}, n_γ from the 10% of events with lowest energy in the hodoscope ($E < 2.5$ mips).

		n_γ								
		0	1	2	3	4	5	6	7	8
	0	84513	9609	1034	138	27	4	1	0	0
	1	27050	3527	478	68	11	1	0	0	0
	2	4737	796	126	14	4	0	1	0	0
	3	737	171	22	8	1	0	0	0	0
n_{ch}	4	98	22	1	1	0	0	0	0	0
	5	14	6	0	0	0	0	0	0	0
	6	4	0	0	0	0	0	0	0	0
	7	0	0	0	0	0	0	0	0	0
	8	0	0	0	0	0	0	0	0	0

numbers of events, $N(n_{ch},n_\gamma)$, in which n_{ch} charged particles and n_γ converted gammas coming from the collision vertex were observed within the acceptance of the detector. The goal of a DCC search is to use these measured probability distributions to identify, or place limits on, a component of multiparticle production arising from disoriented chiral condensates, or other mechanisms leading to anomalous charged-particle–photon joint multiplicity distributions.

As should be clear from the preceding sections, MiniMax faces a number of challenges in carrying out this analysis. These include the following:

(a) The MiniMax acceptance is small, so that it is improbable that both γ's from a π^0 enter the detector acceptance.

(b) The conversion efficiency per γ is about 50%.

(c) Not all γ's come from π^0's.

(d) Not all charged tracks come from $\pi^\pm$'s.

(e) Because of the small acceptance, the multiplicities are rather low, so that statistical fluctuations are very important.

(f) Detection efficiencies for charged tracks and γ's are not the same and are not fully known.

(g) The efficiency for triggering when no charged track or converted γ is produced within our acceptance is relatively low and different from that for events in which at least one charged particle or converted γ is detected.

Nevertheless, we have identified observables which are robust in the sense that, even in the presence of large (un-

TABLE VI. Number of events with a given n_{ch}, n_γ from the 10% of events with highest energy in the hodoscope ($E > 34$ mips).

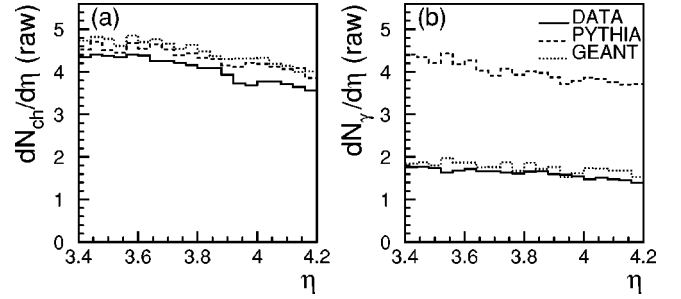|		n_γ								
		0	1	2	3	4	5	6	7	8
	0	59926	11399	1748	281	55	10	0	2	0
	1	33686	7668	1450	275	36	7	1	0	0
	2	10924	2905	595	117	24	7	0	0	0
	3	2705	851	169	39	10	1	0	0	0
n_{ch}	4	575	183	42	7	0	0	0	0	0
	5	112	31	10	1	0	0	0	0	0
	6	16	11	1	0	0	0	0	0	0
	7	2	1	0	0	0	0	0	0	0
	8	0	0	0	0	0	0	0	0	0

FIG. 8. Raw distributions of the pseudorapidity distributions of charged and neutral particles. The curve labelled ''PYTHIA'' refers to simulated events produced by the PYTHIA event generator. These events were then propagated through the GEANT detector simulation and reconstruction algorithms. These results are labelled ''GEANT.'' The large shift between ''PYTHIA'' and ''GEANT'' for the photon distribution is largely due to the conversion probability. The observed data, uncorrected for detection and trigger efficiencies are plotted as ''DATA.'' The close agreement between the ''DATA'' and ''GEANT'' curves validates the simulation procedure and our understanding of the analysis and cuts.

correlated) efficiency corrections and of convolutions from distributions of produced π^0's to those of observed γ's, the observables take very different values for pure DCC's and for generic particle production [6]. Each such observable is a ratio, collectively referred to as R, of certain bivariate normalized factorial moments, which has many desirable properties, including the following:

(1) The R's are not sensitive to the form of the parent pion multiplicity distribution.

(2) The R's are independent of the detection efficiency for finding charged tracks, provided this efficiency is not, for example, momentum dependent or correlated with other variables such as total multiplicity or background level.

(3) Some of the R's are also independent of the γ efficiencies in the same sense as above. In the remaining cases, the R's depend only upon one parameter, ξ, which reflects the relative probability of both photons from a π^0 being detected in the same event.

(4) In all cases R is independent of the magnitude of the null trigger efficiency; see comment (g) above.

(5) The ratios R possess definite and very different values for pure generic and pure DCC pion production.

The idealizations implicit in the realization of properties (1)–(5) include the assumptions that particles other than pions can be ignored, that there is no misidentification of charged particles with photons, and that the production process can be modeled as a two-step process, with a parent-pion multiplicity distribution posited, followed by a particular charged-neutral partitioning of that population by, e.g., a binomial or DCC distribution function. In addition, there is the vital assumption that detection efficiencies for finding a $\pi^\pm$ or γ do not depend upon the nature of the rest of the event.

The validity of these idealizations, and the utility of the robust observables, has been studied in the context of the MiniMax Monte Carlo simulations, and their utility is confirmed in this context [6]. We thus use the robust observables

as the basis for our analysis in the remainder of this paper. It is important to note, however, that some information is lost in this procedure. While we will be sensitive to the presence of DCC, we will make no attempt to unfold the parent distribution of charged and neutral pions, since this would require detailed knowledge of the detection efficiencies for charged tracks and γ's.

B. Factorial moments and robust observables

In analyses of multiparticle distributions, it is frequently useful to work in terms of factorial moments, rather than probability distributions. For example, in standard analyses of charged particle distributions, rather than work with $P(N)$, the probability of observing N charged particles, it is frequently more useful to work with the normalized factorial moments

$$F_i \equiv \frac{\langle N(N-1)\cdots(N-i+1)\rangle}{\langle N \rangle^i}. \tag{2}$$

Part of the utility of these variables arises from the fact that they are unity if the parent distribution $P(N)$ is Poisson, thus essentially removing statistical fluctuations.

In order to search for DCC, the usual multi-particle formalism needs to be extended to bivariate distributions. For the purposes of the MiniMax analysis, this is given by

$$F_{i,j} = \frac{\langle n_{ch}(n_{ch}-1)\cdots(n_{ch}-i+1)n_\gamma(n_\gamma-1)\cdots(n_\gamma-j+1)\rangle}{\langle n_{ch}\rangle^i \langle n_\gamma \rangle^j}. \tag{3}$$

While the normalized bivariate factorial moments are interesting in their own right, particular ratios, R, of them are remarkably robust. In particular, the quantities

$$r_{i,1} = \frac{F_{i,1}}{F_{i+1,0}} \tag{4}$$

are robust in the sense outlined above, including independence of both charged and gamma detection efficiencies. Moreover, it can be shown that, for all $i \geq 1$,

$$r_{i,1}(\text{generic}) = 1,$$

$$r_{i,1}(\text{DCC}) = \frac{1}{i+1}, \tag{5}$$

where ''generic'' indicates the presence of a binomial distribution, and ''DCC'' indicates a pure-DCC joint probability distribution. Evidently, the observables go a long way towards rendering many systematic errors quite harmless to the DCC analysis.

As noted above, these predictions have been tested in the context of the MiniMax Monte Carlo simulation. The combinatorial tracker yields values of $r_{1,1} = 1.02 \pm 0.02$ when minimum bias PYTHIA events are put through the full detector simulation and analysis chain. The combinatorial tracker also results in a value of $r_{1,1} = 0.58 \pm 0.01$ when run on a ''pure'' DCC, indicating that the various idealizations made in deriving the robust observables are indeed reasonably robust.

The u-v tracker, developed independently of the vertex-finding algorithms, has been seen above to have systematic differences from the combinatorial tracker in its performance. This is reflected in the values it yields in the computation of the robust observables, too. In particular, the u-v tracker yields values of $r_{1,1} = 1.13 \pm 0.03$ when minimum bias PYTHIA events are put through the full detector simula-

tion and analysis chain. The u-v tracker also results in a value of $r_{1,1} = 0.66 \pm 0.02$ when run on a ''pure'' DCC. Both values are higher than expected, suggesting that the u-v tracker creates correlations between charged particles and photons in ways that are not well understood. It is for this reason that we report the results of this algorithm, for it provides an estimate of unknown systematic effects. Nevertheless, it is important in what follows to note that the u-v tracker still sees a significant difference in the values of the robust observables when a DCC is present.

V. RESULTS

A. Minimum bias data

The observed joint frequency distribution for charged particles and converted photons for the 1.3×10^6 events tabulated in Table I can be used to calculate the factorial moments and the $r_{i,j}$. The results are tabulated in Table VII. The lower-order $r_{i,1}$ are close to what is expected for a binomial distribution ($r_{i,1} = 1$). The higher-order ratios are weighted towards bins of $\mathcal{N}(n_{ch}, n_\gamma)$ which are statistically limited, and therefore the deviations from unity are not very significant. While the $r_{i,1}$ are robust in the sense defined in Sec. IV, this is not true of the $r_{i,j}, j > 1$ (see [6]). We have nevertheless tabulated these results for completeness, though they are not useful for the present analysis. The u-v tracker yields significantly higher values, consistent with its performance on the Monte Carlo simulation. In any case, the ratios are not smaller than one as would be expected for a contribution from a DCC. We therefore conclude that the analyzed events appear to be consistent with production by only generic mechanisms.

B. Events with diffractive and forward antinucleon tags

The scintillation counters in the vicinity of the kicker magnets at $z \sim -60$ m were used to tag events (''diffractive-

TABLE VII. Values of $r_{i,j}$ for all Pb-in events and for those with upstream tags. Only the $r_{i,1}$ are robust; the other quantities are tabulated for completeness. The entries in a given column are not statistically independent. The last three rows are calculated using the u-v tracker; all others are results from the combinatorial tracker. No. events refers to the number of raw events put through the respective trackers.

	All events	Diffractive $\bar{p}$	Forward $\bar{n}$	Forward $\bar{p}$
No. events	1383336	19180	24757	38112
$\langle n_{ch}\rangle$	0.4843±0.0006	0.401±0.005	0.417±0.004	0.436±0.004
$\langle n_\gamma\rangle$	0.1923±0.0004	0.166±0.003	0.171±0.003	0.181±0.002
$\langle n_{ch}(n_{ch}-1)\rangle$	0.2858±0.0010	0.187±0.007	0.208±0.006	0.225±0.005
$\langle n_{ch}n_\gamma\rangle$	0.1165±0.0005	0.083±0.003	0.089±0.003	0.100±0.003
$r(1,1)$	1.026±0.004	1.07±0.04	1.04±0.03	1.07±0.03
$r(2,1)$	1.035±0.010	1.17±0.12	1.05±0.09	1.11±0.07
$r(3,1)$	1.059±0.027	1.34±0.32	1.29±0.22	1.18±0.18
$r(4,1)$	1.118±0.065	1.77±0.66	2.40±0.68	1.38±0.44
$r(5,1)$	1.310±0.151			1.74±0.92
$r(6,1)$	1.904±0.382			
$r(0,2)$	1.586±0.010	1.70±0.10	1.66±0.08	1.66±0.06
$r(1,2)$	1.573±0.022	1.70±0.25	1.63±0.17	1.65±0.16
$r(2,2)$	1.556±0.053	2.08±0.73	1.71±0.40	1.87±0.47
$r(0,3)$	3.420±0.082	3.64±0.72	3.47±0.63	3.31±0.41
$r(1,3)$	3.165±0.129	3.49±1.35	2.98±0.88	3.16±0.99
$r(0,4)$	9.251±0.683	7.65±3.45	8.56±3.82	6.11±1.79
No. events	242959	22477	29026	44404
$r(1,1)_{uv}$	1.140±0.009	1.17±0.04	1.18±0.03	1.19±0.02
$r(2,1)_{uv}$	1.281±0.026	1.33±0.11	1.45±0.09	1.35±0.08
$r(3,1)_{uv}$	1.506±0.076	1.62±0.32	1.41±0.35	1.36±0.22

$\bar{p}$'' events) in which an antiproton of $x\sim0.9$ was produced and showered into the kicker magnets. The means $\langle n_{ch}\rangle$ and $\langle n_\gamma\rangle$ are lower for such events, as would be expected for a diffractive process, where a large fraction of the total energy is carried away by the beam remnant, and the charged-charged and charged-gamma correlations are correspondingly lower. Table VIII reports these values, as well as the $r_{i,j}$ for the diffractive-$\bar{p}$ events.

The upstream hadronic calorimeters at $z\approx-25$ m are used to tag events with $\bar{p}$'s with $x_F\sim0.5$ (forward-$\bar{p}$ tags) and small-angle $\bar{n}$'s. Differences related to isospin exchange in diffractive events might be apparent in comparisons be-

tween events with an $\bar{n}$ and those with a $\bar{p}$. The moments and $r_{i,j}$ are also listed in Table VII. The mean number of particles found is higher than that in events with the diffractive $\bar{p}$, but lower than in the total sample of events, and is lower for the tag on forward $\bar{n}$'s than for forward $\bar{p}$'s of half the beam momentum, as is consistent with energy conservation.

The $r_{i,j}$ values for these diffractive and forward antinucleon tagged events do not differ significantly from the values for the total sample. Therefore, we conclude that there is no evidence for more DCC production in events with diffractive or forward antinucleon tags, which offers no support

TABLE VIII. Mean multiplicities and robust observables for bins of hodoscope multiplicities each containing 10% of the events. The hodoscope multiplicity increases with increasing bin number 1–10.

| Bin	$\langle n_{ch}\rangle$	$\langle n_\gamma\rangle$	$r_{1,1}$	$r_{2,1}$	$r_{3,1}$
1	0.345±0.002	0.138±0.001	1.03±0.02	1.01±0.05	0.91±0.13
2	0.390±0.002	0.159±0.001	1.03±0.01	1.07±0.04	1.22±0.13
3	0.419±0.002	0.168±0.001	1.04±0.01	1.07±0.04	1.13±0.10
4	0.447±0.002	0.179±0.001	1.03±0.01	1.04±0.04	1.06±0.10
5	0.471±0.002	0.189±0.001	1.03±0.01	1.05±0.04	1.10±0.10
6	0.499±0.002	0.196±0.001	1.03±0.01	1.07±0.04	1.17±0.09
7	0.516±0.002	0.206±0.001	1.03±0.01	1.06±0.03	1.11±0.09
8	0.549±0.002	0.218±0.001	1.01±0.01	1.01±0.03	1.08±0.07
9	0.587±0.002	0.230±0.001	1.02±0.01	1.00±0.03	0.96±0.06
10	0.646±0.002	0.249±0.001	1.04±0.01	1.04±0.02	1.03±0.05
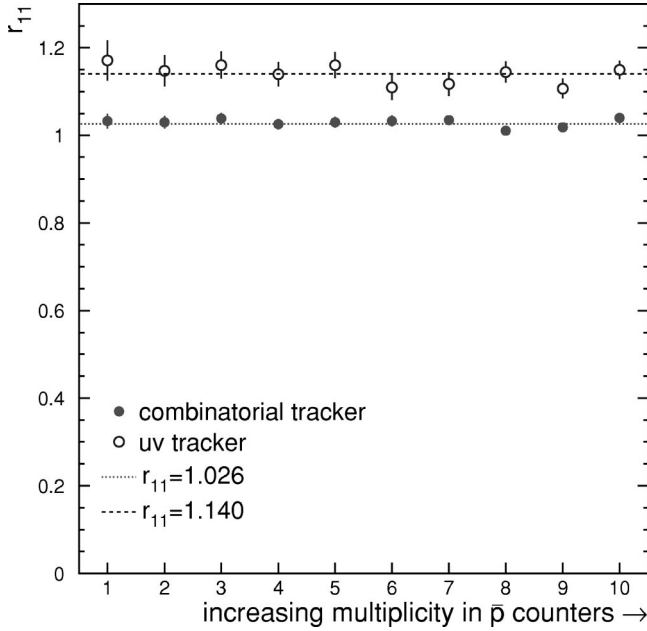
FIG. 9. The robust observable $r_{1,1}$, for both the combinatorial and the u-v trackers, as a function of multiplicity in the scintillator hodoscope. The multiplicity bins are defined as in Fig. 7. The horizontal lines indicate the values of $r_{1,1}$ for all events (not separated into multiplicity bins): $r_{1,1}=1.026\pm0.004$ for the combinatorial tracking algorithm and $r_{1,1}=1.140\pm0.009$ for the u-v tracking algorithm.

to the conjecture that Centauro events are related to DCC's and are diffractive in nature.

C. Events with an opposite side multiplicity tag

As can be seen from Fig. 7, there is a long range correlation in multiplicity which permits us to tag mean multiplicities within the acceptance of the tracking telescope by cutting on the multiplicity observed in the scintillator hodoscope even though it is 7 units of pseudorapidity away. This provides a powerful tool for checking the hypothesis that DCC content is multiplicity dependent.

Figure 9 illustrates the dependence of $r_{1,1}$ on multiplicity. The horizontal lines in the figure indicate the values of $r_{1,1}$ calculated from the entire data set. Testing the hypothesis that the values of $r_{1,1}$ in each of the ten multiplicity bins all come from the same parent value of $r_{1,1}$ (that for the entire data set) yields $\chi^2=7.06$ for the combinatorial tracker and $\chi^2=5.58$ for the u-v tracker. Fitting to a line gives a small, statistically irrelevant, slope: $r_{1,1}=(1.0320\pm0.0093)-(0.0006\pm0.0013)\times$(multiplicity bin No.) with $\chi^2=7.04$ for the combinatorial tracker and $r_{1,1}=(1.1563\pm0.0227)-(0.0029\pm0.0032)\times$(multiplicity bin No.) with $\chi^2=4.62$. Thus, while there is a significant difference between the two trackers in the absolute value of $r_{1,1}$, neither tracker shows any indication of a multiplicity dependence in $r_{1,1}$.

We conclude that there is no evidence of a multiplicity dependence in the partitioning of pions into charged and neutral species, and hence no evidence for a multiplicity dependence in DCC production.

VI. CONCLUSIONS

The principal goals of test/experiment T864 were (1) to determine whether spectrometers such as ours could be triggered and would survive the severe background conditions present in the far-forward direction of a high-energy collider environment, (2) to search for DCC's, (3) to search for exotic phenomena such as Centauro events, and (4) to provide data on inclusive spectra, correlations, and multiplicity distributions in a previously unexplored region of phase space.

At the time of the proposal, the first goal of the initiative was a very serious issue. There was very little working experience, and what did exist was not encouraging. But Mini-Max ran successfully with many different detector configurations for a period of about two years. Much was learned which should prove useful for the operation and design of future detectors in the forward region. More than 1.3×10^6 events from clean low-luminosity runs with the detector functioning properly have been analyzed for the work presented here.

With regard to our DCC search, we have seen no evidence for the presence of DCC's. Robust observables sensitive to the partition of pions into charged and neutral species have been found to good accuracy to not depend upon associated multiplicity or upon the presence or absence of a leading nucleon or of a diffractive proton. These results have been obtained from a data-driven analysis method developed by the collaboration, a method which has general applicability to DCC searches [13].

In order to determine the limits on DCC production implied by our measurements, we have to face two issues: the determination of a lower bound on the possible values of the robust observables consistent with our data, and the dependence of the robust observables on various models for DCC production.

The question of a lower bound on the robust observables is complicated by the discrepancy between the values resulting from our two tracking algorithms. For the statistically most significant observable, $r_{1,1}$, the combinatorial tracker yielded a value of $r_{1,1}=1.026\pm0.004$ while the u-v tracker yielded a value of $r_{1,1}=1.140\pm0.009$. This discrepancy is also present in the respective results of the Monte Carlo simulations: the combinatorial tracker yielded a value of $r_{1,1}=1.02\pm0.02$, while the u-v tracker yielded $r_{1,1}=1.13\pm0.03$.

We believe that a realistic approach to this discrepancy is to normalize the results of each tracker on the data to the results on the Monte Carlo simulation. For the combinatorial tracker, this yields

$$r^{normalized}=\frac{r_{1,1}^{data}}{r_{1,1}^{MC}}=1.01\pm0.02 \quad \text{(combinatorial tracker)}.$$

(6)

The corresponding one-sided lower limit at the 95% confidence level (1.645σ) is $r^{normalized}\geqslant0.973$. The u-v tracker yields

$$r^{normalized} = \frac{r_{1,1}^{data}}{r_{1,1}^{MC}} = 1.01 \pm 0.03 \quad (u\text{-}v \text{ tracker}), \quad (7)$$

with a one-sided lower limit at the 95% confidence level of $r^{normalized} \geqslant 0.963$.

These limits are consistent with generic, binomial-distribution partition of pions into charged and neutral species. While the robust observables, being independent of detection efficiencies, do not permit the determination of the neutral fraction, we note that Fig. 8 indicates that the normalization of the observed inclusive measurements of gam-

mas and charged particles agree with PYTHIA+GEANT simulations at roughly the 10% level.

The limits on DCC production implied by these lower bounds on the robust observables are strongly dependent on the model for DCC production one uses. The nature of this model dependence has been described in detail in our previous paper [6]. Two extreme cases illustrate some of the issues: one (''exclusive production'') where a given event is described by either DCC or generic production and the other (''associated production'') where DCC production is proportional to generic production.

In the case of associated production,

$$r_{1,1}^{assoc}(\lambda) = \frac{\left[(1-\lambda)^2 \hat{f}(1-\hat{f}) + \frac{1}{3}\lambda(1-\lambda)(1+\hat{f}) + \frac{2}{15}\lambda^2 \right]\left[(1-\lambda)(1-\hat{f}) + \frac{2}{3}\lambda \right]}{\left[(1-\lambda)^2(1-\hat{f})^2 + \frac{4}{3}\lambda(1-\lambda)(1-\hat{f}) + \frac{8}{15}\lambda^2 \right]\left[(1-\lambda)\hat{f} + \frac{1}{3}\lambda \right]}, \quad (8)$$

where $\lambda = \langle N \rangle_{DCC} / \langle N \rangle_{generic}$ and $\hat{f}$ is the mean fraction of π^0's in generic production, which we take here to be 1/3. In this case, one can solve for an upper limit on λ in terms of $r_{1,1}^{lower\ limit}$:

$$\lambda \leqslant \sqrt{\frac{5(1 - r_{1,1}^{lower\ limit})}{r_{1,1}^{lower\ limit} + 2}}. \quad (9)$$

For this model of DCC production, we thus find an upper limit on DCC production of $\lambda \leqslant 0.21$ based on the results of the combinatorial tracker.

In the case of exclusive production,

$$r_{1,1}^{excl}(\lambda) = \frac{\left[1 + \lambda\left(\frac{2}{15\hat{f}(1-\hat{f})} \frac{\langle N(N-1) \rangle^{DCC}}{\langle N(N-1) \rangle^{Gen}} - 1 \right) \right]\left[1 + \lambda\left(\frac{2}{3(1-\hat{f})} \frac{\langle N \rangle^{DCC}}{\langle N \rangle^{Gen}} - 1 \right) \right]}{\left[1 + \lambda\left(\frac{8}{15(1-\hat{f})^2} \frac{\langle N(N-1) \rangle^{DCC}}{\langle N(N-1) \rangle^{Gen}} - 1 \right) \right]\left[1 + \lambda\left(\frac{1}{3\hat{f}} \frac{\langle N \rangle^{DCC}}{\langle N \rangle^{Gen}} - 1 \right) \right]}, \quad (10)$$

where λ is the probability that an event will be a DCC. In general, this expression depends on ratios of the first and second moments of the parent DCC and generic multiplicity distributions, as well as on $\hat{f}$. Illustrative bounds follow from assuming that the parent distributions are the same, and that $\hat{f} = 1/3$. In this case, one can again solve for an upper limit on λ in terms of our lower limits on $r_{1,1}$:

$$\lambda \leqslant \frac{5(1 - r_{1,1}^{lower\ limit})}{r_{1,1}^{lower\ limit} + 2}. \quad (11)$$

For this model of DCC production, we thus find an upper limit on DCC production of $\lambda \leqslant 0.05$.

A third model, independent production, in which DCC production occurs independently of generic production, was also discussed in our earlier paper. As noted there, the precise value of the robust observables depends in this case on the details of both generic and DCC production, so that analytic formulas such as those we have just considered are of

less utility. In our earlier paper, we have reported the results for a series of Monte Carlo simulations in which a varying amounts of DCC are added to generic events. The parameters of the DCC generator used for these simulations corresponded to domains of DCC with energy density comparable to that of generic production, and $\langle p_t \rangle \sim 140$ MeV. Interpolating from the results reported in Table I of [6], we deduce limits on DCC production in this scenario of about 5%.

Similar analyses (and conclusions) are possible for the data subsets defined by the diffractive and forward antinucleon tags, and for events with opposite side multiplicity tags. Indeed, there is no evidence of a multiplicity dependence in the robust observables. (See Fig. 9). We believe that this, together with the overall agreement between data and simulations suggested by Fig. 8, goes far towards validating our results.

Detailed discussion of the third and fourth goals of the experiment is beyond the scope of this paper. We have of course made preliminary searches for exotic phenomena, and

have seen no evidence for them. A major reason for not reporting them here in more detail is that about 1% of our triggers have so many hits in the chambers (e.g. $N_{hits} > 1200$, or a mean occupancy per wire of more than 40%) that the event is almost completely unanalyzable. One may therefore argue that the exotic events might be only present in this subset of data. We have some circumstantial evidence against this argument, because in many of these very cluttered events there are portions of the acceptance which are relatively clean, and in those regions no unusual behavior is indicated.

Were Centauro behavior present, we would expect to see an excess of events with high charged multiplicity; no tail in the multiplicity distribution is observed. The JACEE Collaboration has exhibited a highly unusual event containing high multiplicity and a gamma ray excess [14]. Our joint distribution in gammas and charged tracks significantly limits this behavior, provided the gamma ray efficiency as determined in Fig. 4 can be extrapolated further in multiplicity. But we again emphasize that in all these cases these limits would be only valid if the background problem described in the previous paragraph is ignored.

With regard to the fourth goal of the experiment, measurements of $dN_{ch}/d\eta$ and $dN_\gamma/d\eta$ have been made in a previously unexplored region of phase space (cf. Fig. 8). Fully normalized distributions, which take into account detection and trigger efficiencies and fake tracks, have not yet been derived. Further work on modeling fake tracks in the data is necessary before this can be done.

This test/experiment was an extremely modest endeavor. Many lessons were learned, which may apply to more ambitious efforts in the future. Some are obvious: it would be beneficial to have larger acceptance, together with momentum measurement of both charged particles and gammas. With regard to the serious backgrounds in the forward direction, miniaturization of the detection elements with finer spatial resolution, in both tracking and in calorimetry, greatly reduces the difficulties. An example of a proposed detector with such properties is the FELIX initiative for the LHC [15].

[1] For descriptions and preliminary results of the MiniMax experiment (T-864) see The MiniMax Collaboration (J. D. Bjorken and C. C. Taylor, co-spokespersons), Fermilab Proposal T-864, 1993; J. D. Bjorken, K. L. Kowalski, and C. C. Taylor, in Proceedings of the Workshop on Physics at Current Accelerators and the Supercollider, edited by J. L. Hewett, A. R. White, and D. Zeppenfeld, ANL Report No. 93-92, Argonne, 1993, hep-ph/9309235, p. 73; J. D. Bjorken, in *23rd International Symposium on Multiparticle Dynamics (1993)*, Proceedings, Aspen, Colorado, edited by M. Block and A. White (World Scientific, Singapore, 1994); C. C. Taylor, in *Proceedings of the International Conference on Elastic and Diffractive Scattering*, edited by H. M. Fried, K. Kang, and C.-I Tan (World Scientific, Singapore, 1994), p. 348; in *Hot Hadronic Matter: Theory and Experiment*, edited by J. Letessier *et al.* (Plenum Press, New York, 1995), p. 503; M. Convery *et al.*, in Proceedings of the 24th International Cosmic Ray Conference, Rome, 1995, edited by N. Iucci and E. Lamanna, Invited Papers, p. 1045 [Nuovo Cimento C **19** (1996)]; L. W. Jones *et al.*, in *Proceedings of the 24th Cosmic Ray Conference*, Rome, 1995 (Istituto Nazionale di Fisica Nucleare, Roma, Italy, 1996), Vol. 1, p. 886; M. E. Convery *et al.*, Bull. Am. Phys. Soc. **41**, 902 (1996); W. L. Davis *et al.*, *ibid.* **41**, 938 (1996); J. D. Bjorken, in *Proceedings of the 7th International Workshop on Multiparticle Correlations ''Correlations and Fluctuations,''* Nijmigen, The Netherlands, 1996, edited by W. Kittel (World Scientific, Singapore, 1997); C. C. Taylor, in Proceedings of the RHIC Summer Studies '96 Workshop, Brookhaven, New York, 1996, edited by D. E. Kahana and Y. Pang, p. 329; J. Streets, in *Proceedings of the DPF Meeting*, Minneapolis, 1996 (World Scientific, Singapore, 1997); L. W. Jones *et al.*, in *Proceedings of the 25th International Cosmic Ray Conference*, Durban, South Africa, 1997 (Potchefstroomse Univ. Press, Potchefstroom, South Africa, 1998), Vol. 6, p. 29.

[2] M. E. Convery, Ph.D. Thesis, Case Western Reserve University, 1997, hep-ex/9801020.

[3] Early papers include A. A. Anselm, Phys. Lett. B **217**, 169 (1989); A. A. Anselm and M. G. Ryskin, *ibid.* **266**, 482 (1991); J. D. Bjorken, Int. J. Mod. Phys. A **7**, 4189 (1992); Acta Phys. Pol. B **23**, 561 (1992); J-P. Blaizot and A. Krzywicki, Phys. Rev. D **46**, 246 (1992); K. Rajagopal and F. Wilczek, Nucl. Phys. **B399**, 395 (1993).

[4] For recent reviews, see K. Rajagopal, in *Quark-Gluon Plasma 2*, edited by R. Hwa (World Scientific, Singapore, 1995), p. 484; J-P. Blaizot and A. Krzywicki, Acta Phys. Pol. B **27**, 1687 (1996); K. Ragjagopal, talk at the International Workshop on QCD Phase Transitions, 1997, Hirschegg, Austria, hep-ph/970-3258; J. D. Bjorken, in Proceedings of the 1997 Zakopane School [Acta Phys. Pol. B **28**, 2773 (1997)].

[5] Papers discussing other mechanisms for the $1/\sqrt{f}$ distribution include D. Horn and R. Silver, Ann. Phys. (N.Y.) **66**, 509

(1971); I. V. Andreev, Pis'ma Zh. Eksp. Teor. Fiz. **33**, 384 (1981) [JETP Lett. **33**, 367 (1981)]; V. Karmanov and A. Kudrjavtsev, Report No. ITEP-88, 1983; S. Pratt, Phys. Lett. B **301**, 159 (1993); R. D. Amado *et al.*, Phys. Rev. Lett. **72**, 970 (1994); M. Martinis, V. Mikuta-Martinis, A. Švarc, and J. Črnugelj, Phys. Rev. D **51**, 2482 (1995); Phys. Rev. C **52**, 1073 (1995); Fiz. B **133**, 197 (1994).

[6] MiniMax Collaboration, T. C. Brooks *et al.*, Phys. Rev. D **55**, 5667 (1997).

[7] P. R. Bevington *et al.*, Nucl. Instrum. Methods **129**, 373 (1975).

[8] F. Abe *et al.*, Phys. Rev. D **50**, 5550 (1994); **50**, 5518 (1994); **50**, 5535 (1994).

[9] ALICE Collaboration, Report No. CERN/LHCC/96-32, LHCC/P3/Addendum 1, 1996, pp. 19–22.

[10] H.-U. Bengtsson and T. Sjostrand, Comput. Phys. Commun. **46**, 43 (1987).

[11] GEANT—Detector Description and Simulation Tool, CERN Program Library Long Writeup W5013, Application Software Group, Computing and Networks Division, CERN, Geneva, Switzerland, 1993.

[12] K. Goulianos, Comments Nucl. Part. Phys. **17**, 195 (1987); J. D. Bjorken, K. L. Kowalski, and C. C. Taylor, in Proceedings of the Workshop on Physics at Current Accelerators and the Supercollider, edited by J. L. Hewett, A. R. White, and D. Zeppenfeld, ANL Report No. 93-92, Argonne, 1993, p. 73, hep-ph/9309235.

[13] WA98 Collaboration, M. M. Aggarwal *et al.*, Phys. Lett. B **420**, 169 (1998); WA98 Collaboration, Tapank K. Nayak *et al.*, Nucl. Phys. **A638**, 249c (1998).

[14] J. J. Lord and J. Iwai, Paper No. 515, presented at the International Conference on High Energy Physics, Dallas, 1992; H. Wilczynski *et al.*, in Proceedings of the XXIV International Cosmic Ray Conference, HE Sessions, Rome, 1995, Vol. 1, p. 1.

[15] FELIX Collaboration, ''FELIX, A full acceptance detector for the LHC,'' Report No. CERN/LHCC 97-45, LHCC/I10, 1997.